

Fabrication of Methyl Parathion Electrochemical Sensor Based on Modified Glassy Carbon Electrode with Graphitized and Carboxylated Multi-Walled Carbon Nanotubes Decorated with Zirconia Nanoparticles

Gan Zhu, Yaqi Zhang, Yunhang Liu, Meimei Guo, Mingming Zhang, Tingting Wu, Yongfeng Li, Hongyuan Zhao*

Research Center for Advanced Materials and Electrochemical Technology, School of Mechanical and Electrical Engineering, Henan Institute of Science and Technology, Xinxiang 453003, China

*E-mail: hongyuanzhao@126.com

Received: 3 March 2022 / Accepted: 23 April 2022 / Published: 7 May 2022

Herein, we modified the glassy carbon electrode (GCE) by using the nanocomposite of graphitized and carboxylated multi-walled carbon nanotubes (GR-MWCNTs-COOH) and zirconia (ZrO_2) nanoparticles for the fabrication of GR-MWCNTs-COOH/ ZrO_2 /GCE sensor. GR-MWCNTs-COOH had high electrical conductivity, large specific surface area, and good hydrophilicity. ZrO_2 nanoparticles possessed strong affinity toward the phosphorus groups on methyl parathion (MP) molecules, which contributes to the enrichment of MP on the modified GCE surface. The fabricated GR-MWCNTs-COOH/ ZrO_2 /GCE sensor exhibited excellent electrochemical sensing performance for the determination of MP due to the synergistic effect of GR-MWCNTs-COOH and ZrO_2 . Under the optimal conditions, the GR-MWCNTs-COOH/ ZrO_2 /GCE sensor could show a low limit of detection of 0.00135 μM in linear MP concentration range of 0.01-10 μM . Moreover, the fabricated sensor presented good reproducibility, repeatability, and selectivity, which could promote the practical application of MP sensor.

Keywords: Graphitized and carboxylated multi-walled carbon nanotubes; Zirconia nanoparticles; Methyl parathion; Glassy carbon electrode; Electrochemical sensor

1. INTRODUCTION

As one kind of organophosphorus pesticides, methyl parathion (MP) was used to ensure the quality of agricultural products in the previous decade years [1, 2]. However, MP residue can cause serious pollution to ecological environment. According to the existing literature [3, 4], MP can inhibition the activity of acetylcholinesterase (AChE), which makes the accumulation of acetylthiocholine. The acetylthiocholine is harmful to the nervous system of human body, which may cause muscle paralysis, heart disease, and even death [5]. Therefore, it is important to develop some simple and efficient methods

to detect the MP pesticide. Nowadays, the determination of MP mainly depends on some traditional detection methods such as gas chromatography (GC) [6], high performance liquid chromatography (HPLC) [7], capillary-liquid chromatography (CLC) [8], and gas chromatography-mass spectroscopy (GC-MS) [9-11]. These methods have several disadvantages such as expensive analysis cost, long sample pretreatment time, and complex professional operation.

It is important to note that electrochemical detection technology not only decrease the analysis cost but also simplify the experimental operation. At present, there are many reported research works about the design of high-performance electrochemical sensors [12-16]. Especially, carbon-based composite materials can significantly enhance the detection performance of electrochemical sensors. It has been reported that different types of carbon nanotubes possess different enhancement effects on the electrochemical performance of electrochemical sensors [17, 18]. Compared with the unfunctionalized MWCNTs, the graphitized multi-walled carbon nanotubes (GR-MWCNTs) can help enhance the electric conductivity of carbon nanotubes due to the high graphitization degree and highly ordered graphitic structure [19, 20], and the carboxylated multi-walled carbon nanotubes (MWCNTs-COOH) can present more uniform dispersion effect due to the hydrophilicity of carboxyl functional groups [21, 22]. Ni et al. reported the GR-MWCNTs-based composite modified GCE sensor, which showed excellent electrochemical sensing determination performance [23]. Li et al. fabricated a novel electrochemical sensor based on the MWCNTs-COOH modified GCE, which achieved more sensitive detection of bisphenol A with lower limit of detection compared to the MWCNTs modified GCE sensor [22]. Therefore, the graphitized and carboxylated multi-walled carbon nanotubes (GR-MWCNTs-COOH) was selected as surface modification material to fabricate the electrochemical sensor for the highly sensitive determination of MP. Furthermore, Prabhu et al. prepared the high-performance electrochemical sensor based on the silica gel modified carbon paste electrode, which was applied for the sensitive detection the linuron with a low limit of detection of 3.94 nM ($S/N=3$) in the concentration range of 1.0-4.5 μM [24]. Wang et al. fabricated the electrochemical sensor modified by the carboxylated single-wall carbon nano-tubes decorated with SiO_2 coated- Nd_2O_3 nanoparticles, which achieved a low limit of detection of 0.70 μM [25]. Upan et al. prepared a screen-printed graphene-carbon paste electrode (SPGE) modified by platinum nanoparticles on carboxylated-graphene oxide (PtNPs/GO-COOH), which presents a good alpha-fetoprotein electrochemical performance with a low limit of detection of 1.22 ng mL^{-1} [26]. Furthermore, Zhao et al. fabricated a novel methyl parathion electrochemical sensor based on the glassy carbon electrode modified by halloysitenanotubes/multi-walled carbon nanotubes nanocomposite, which showed good linear relationship (MP concentration: 0.5-11 μM) and low limit of detection of 0.034 mM [27]. These research works indicated that carbon-based composite materials are extremely meaningful for high-performance electrochemical sensor.

In this work, we modified the glassy carbon electrode (GCE) by using the nanocomposite of graphitized and carboxylated multi-walled carbon nanotubes (GR-MWCNTs-COOH) and zirconia (ZrO_2) nanoparticles for the fabrication of GR-MWCNTs-COOH/ ZrO_2 /GCE sensor, as shown in **Scheme 1**. In our previous paper [28], the β -cyclodextrin modified GR-MWCNTs-COOH nanocomposite enhanced the MP detection performance due to the synergistic effect of β -CD and GR-MWCNTs-COOH. GR-MWCNTs-COOH had high electrical conductivity, large specific surface area, and good hydrophilicity, and β -CD promoted the uniform dispersion of GR-MWCNTs-COOH and

possessed excellent molecular recognition ability for organic molecules. By contrast, ZrO₂ nanoparticles with simple production process and cheap production cost possessed strong affinity toward the phosphorus groups on MP molecules, which contributes to the enrichment of MP on the modified GCE surface [29, 30]. The combination of GR-MWCNTs-COOH and ZrO₂ can make full use of their respective advantages. The fabricated GR-MWCNTs-COOH/ZrO₂/GCE sensor showed good electrochemical sensing performance for the MP determination.

2. EXPERIMENTAL PART

2.1. Materials and reagents

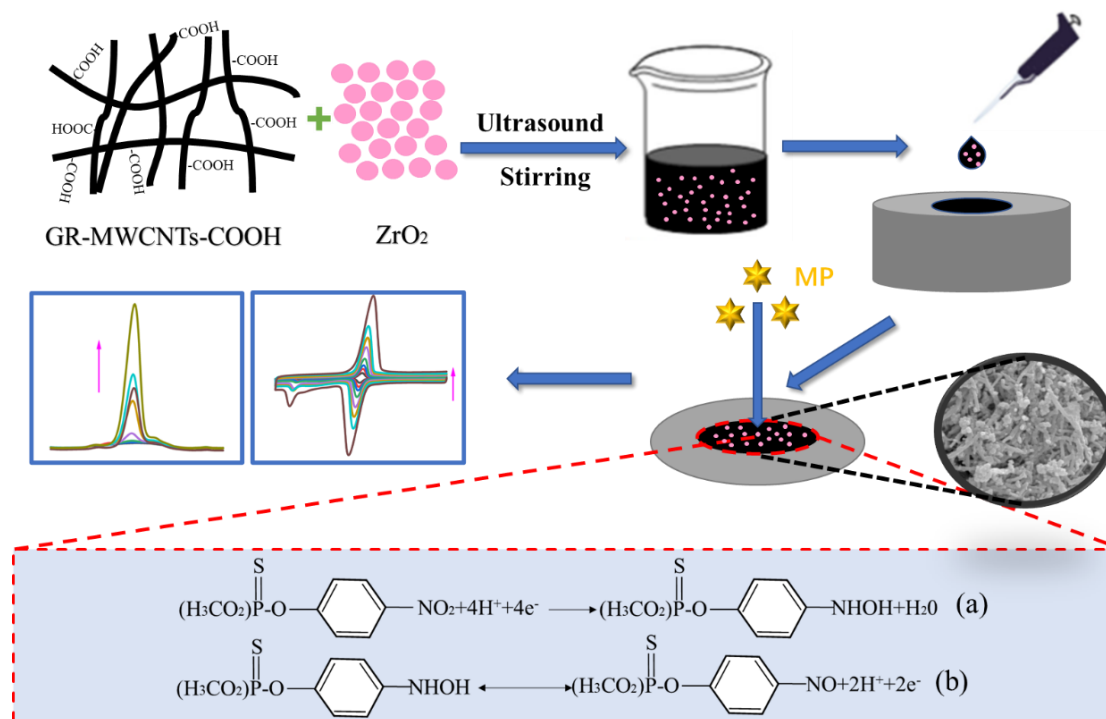
Graphitized and carboxylated multi-walled carbon nanotubes (GR-MWCNTs-COOH), zirconia (ZrO₂) nanoparticles, dimethylformamide (DMF), phosphate, potassium ferricyanide, alcohol and methyl parathion (MP) were provided from Shanghai Aladdin Biochemical Technology Co., Ltd. Alumina powders with different particle sizes were purchased from CH Instruments Ins.

2.2. Preparation of GR-MWCNTs-COOH/ZrO₂/GCE sensors

The GR-MWCNTs-COOH/ZrO₂/GCE sensor was fabricated by a simple drop coating method. 10 mg of GR-MWCNTs-COOH was dissolved in 5 mL of DMF solution with help of ultrasonic dispersion treatment for 60 mins. After that, 45 mg of ZrO₂ nanoparticles were added into the above GR-MWCNTs-COOH suspension followed with the ultrasonic dispersion treatment for 60 mins. And then, a certain amount of GR-MWCNTs-COOH/ZrO₂ mixed solution (5 μ L) was deposited onto the pretreated GCE surface to fabricate the GR-MWCNTs-COOH/ZrO₂/GCE sensor.

2.3. Material characterization

The microstructure and morphology were further explored by Fourier transform infrared (FTIR) spectrum, Raman spectroscopy (RS), X-ray diffraction (XRD) and energy Dispersive X-Ray spectroscopy (EDS). The differential pulse voltammetry (DPV), electrochemical impedance spectroscopy (EIS) and cyclic voltammetry (CV) measurements were performed by CHI660e electrochemical workstation.



Scheme 1. Preparation of GR-MWCNTs-COOH/ZrO₂/GCE sensor for the determination of MP.

3. RESULTS AND DISCUSSION

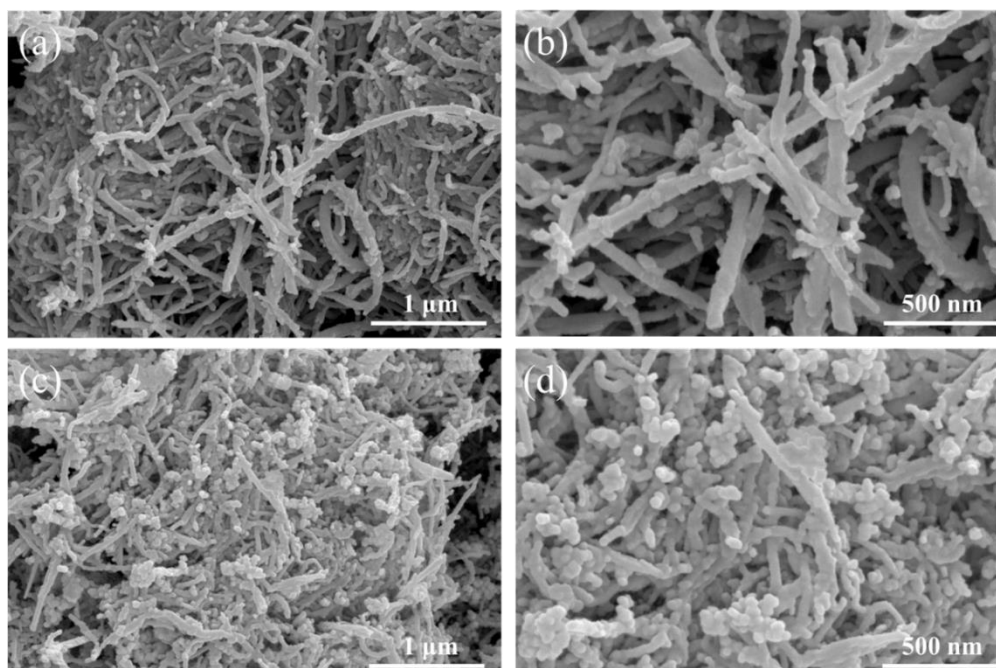


Figure 1. SEM images of (a, b) GR-MWCNTs-COOH and (c, d) GR-MWCNTs-COOH/ZrO₂.

SEM characterization was used to investigate the morphology of the GR-MWCNTs-COOH and GR-MWCNTs-COOH/ZrO₂ samples. It can be seen from **Fig. 1 (a, b)** that the GR-MWCNTs-COOH sample is composed of lots of carbon nanotubes, which form an interconnected three-dimensional network structure.

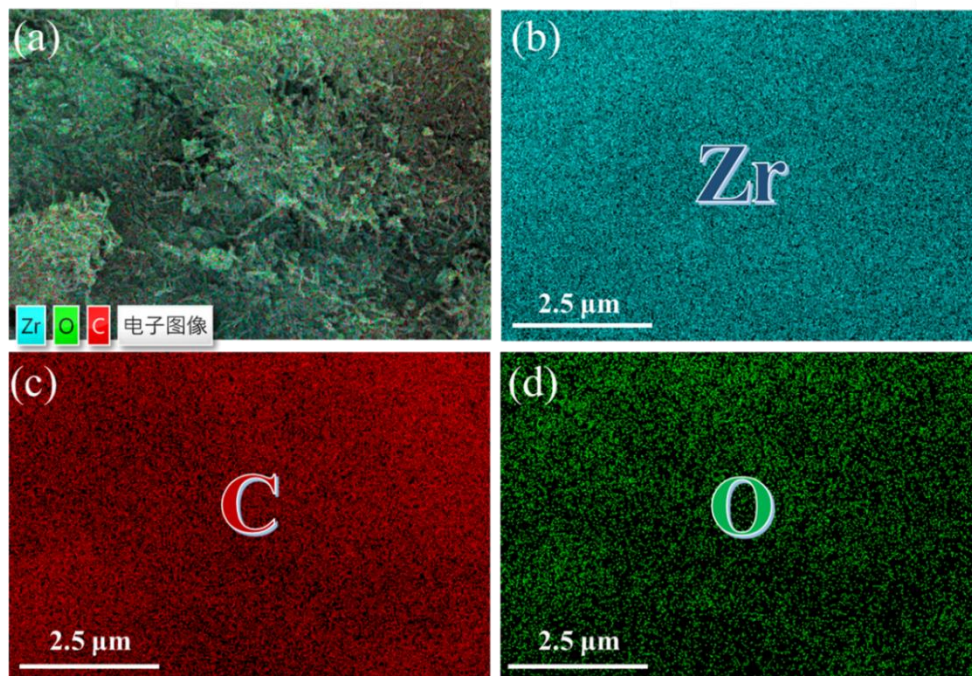


Figure 2. (a) mixed elements mapping image and (b-d) single element images of Zr, C and O.

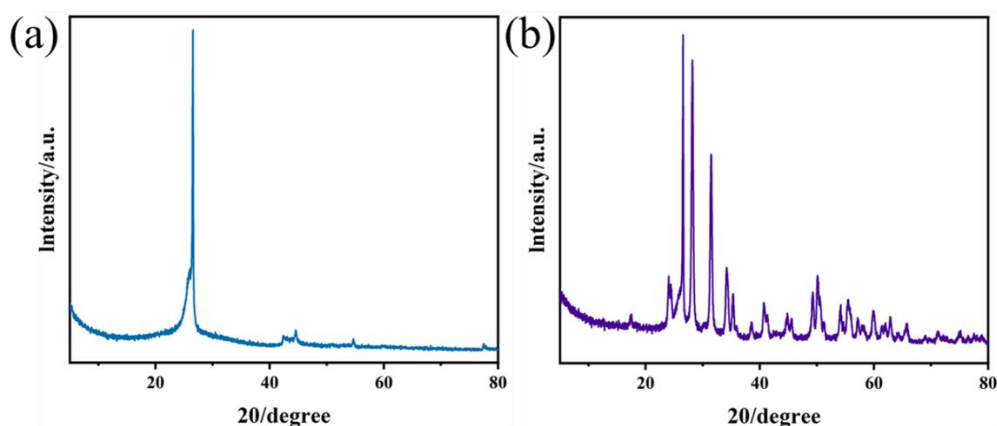


Figure 3. XRD patterns of (a) GR-MWCNTs-COOH and (b) GR-MWCNTs-COOH/ZrO₂.

As shown in **Fig. 1 (c, d)**, ZrO₂ nanoparticles are uniformly dispersed in the interconnected three-dimensional network structure of GR-MWCNTs-COOH. Such mixed microstructure may effectively improve the electrochemical determination performance of GR-MWCNTs-COOH/ZrO₂/GCE sensor

towards MP. The EDX images of the GR-MWCNTs-COOH/ZrO₂ sample shown in **Fig. 2**. **Fig. 2 (a)** shows the mixed elements mapping image of the obtained nanocomposite. **Fig. 2 (b-d)** shows the single element images of Zr, C and O in the GR-MWCNTs-COOH/ZrO₂ sample. It is significant to note that these elements exhibit uniform distribution, which is consistent with mixed elements mapping image shown in **Fig. 2 (a)**.

Fig. 3 (a) shows the XRD pattern of GR-MWCNTs-COOH. It has two obvious characteristic diffraction peaks of carbon nanotubes with strong peak intensity, which suggests the high graphitization degree of carbon material [31]. There are no miscellaneous peak in XRD pattern of GR-MWCNTs-COOH, which suggests the high purity of carbon material. **Fig. 3 (b)** presents the XRD pattern of the obtained GR-MWCNTs-COOH/ZrO₂ nanocomposite. It can be found that the XRD pattern of GR-MWCNTs-COOH/ZrO₂ involves the characteristic diffraction peaks of GR-MWCNTs-COOH. It is important to note that several characteristic diffraction peaks of ZrO₂ can be clearly observed in the XRD pattern of this nanocomposite, which further confirm the successful preparation of the GR-MWCNTs-COOH/ZrO₂ nanocomposite [29, 32, 33].

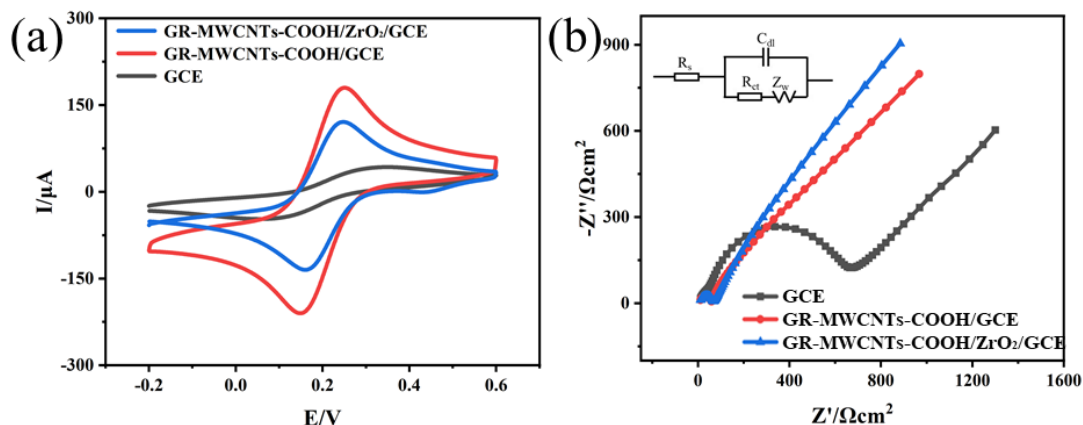


Figure 4. (a) CV curves and (b) Nyquist plots of the bare GCE, GR-MWCNTs-COOH/GCE and GR-MWCNTs-COOH/ZrO₂/GCE sensors at 100 mV s⁻¹ in 5 mM K₃[Fe(CN)₆]/K₄[Fe(CN)₆] solution containing 0.1m KCl.

Fig. 4(a) shows the CV curves of the bare GCE, GR-MWCNTs-COOH/GCE and GR-MWCNTs-COOH/ZrO₂/GCE sensors, and the supporting solution is 5 mM K₃[Fe(CN)₆]/K₄[Fe(CN)₆] containing 0.1 mM KCL. As shown here, the current trend of the bare GCE was relatively flat with no obvious prominent peak, which agrees with the reported results [29, 32]. By contrast, there were distinct redox peaks at the GR-MWCNTs-COOH/GCE and GR-MWCNTs-COOH/ZrO₂/GCE sensors. The corresponding anode peak current and cathode peak value are $I_{pa}=186.3 \mu\text{A}$ and $I_{pc}=-129.21 \mu\text{A}$ for GR-MWCNTs-COOH/GCE sensor. For the GR-MWCNTs-COOH/ZrO₂/GCE sensor, the introduction of ZrO₂ nanoparticles decreases the redox peak values due to the poor electrical conductivity [29]. The corresponding anode peak current and cathode peak value are $I_{pa}=124.4 \mu\text{A}$ and $I_{pc}=-78.67 \mu\text{A}$, respectively. **Fig. 4 (b)** exhibits the Nyquist plots of the bare GCE, GR-MWCNTs-COOH/GCE, and

GR-MWCNTs-COOH/ZrO₂/GCE sensors. The electrochemical impedance spectroscopy (EIS) result illustrates the R_{ct} value of the above sensors. Compared with the large R_{ct} value (663.05 $\Omega \text{ cm}^2$) of the bare GCE sensor, both GR-MWCNTs-COOH/GCE and GR-MWCNTs-COOH/ZrO₂/GCE sensors present low R_{ct} values (48.25 $\Omega \text{ cm}^2$, 56.72 $\Omega \text{ cm}^2$) due to the excellent conductivity property of GR-MWCNTs-COOH.

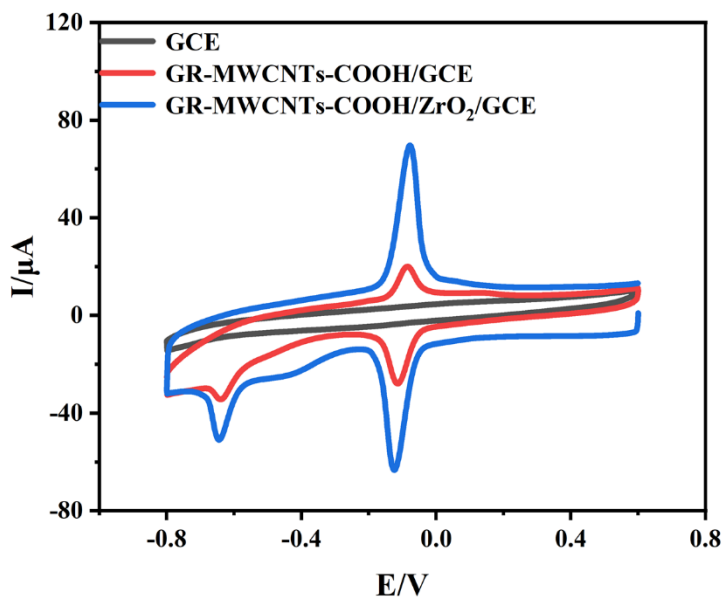


Figure 5. CV curves in 30 μM MP at the bare GCE, GR-MWCNTs-COOH/GCE, and GR-MWCNTs-COOH/ZrO₂/GCE sensors in 0.1 M PBS solution (pH=7.0, Potential range: -0.8-0.6v, Scan rate: 100 mV s^{-1}).

Fig. 5 shows the CV curves of 30 μM MP at the bare GCE, GR-MWCNTs-COOH/GCE, and GR-MWCNTs-COOH/ZrO₂/GCE sensors (pH=7.0, Potential range: -0.8-0.6v, Scan rate: 100 mV s^{-1}). As with the CV curves of the bare GCE shown in **Fig. 4(a)**, the current trend of the bare GCE was relatively flat, which agrees with the previous research work [29, 33]. By contrast, a pair of obvious reversible redox peaks and an irreversible cathode peak appeared in the CV curves of MP at the GR-MWCNTs-COOH/GCE and GR-MWCNTs-COOH/ZrO₂/GCE sensors. For the GR-MWCNTs-COOH/GCE sensor, the corresponding anode peak current value is $I_{pa}=12.84 \mu\text{A}$ and the cathode peak value is $I_{pc}=-21.92 \mu\text{A}$. By contrast, the GR-MWCNTs-COOH/ZrO₂/GCE sensor presents the best MP determination performance with anode peak current value of $I_{pa}=56.61 \mu\text{A}$ and cathode peak value of $I_{pc}=-51.62 \mu\text{A}$. Such high performance was mainly ascribed to the synergistic effect of GR-MWCNTs-COOH and ZrO₂ nanoparticles. GR-MWCNTs-COOH had high electrical conductivity, large specific surface area, and good hydrophilicity, which provide more efficient charge transfer channels and larger electrochemical active area [19-21]; ZrO₂ nanoparticles possessed strong affinity toward the phosphorus groups on MP molecules, which can contribute to the enrichment of MP on the GR-MWCNTs-COOH/ZrO₂/GCE sensor [29, 32].

The pH value is a significant factor for the MP determination. The pH optimization was carried out based on the DPV measurement. **Fig. 6 (a, b)** displays the DPV curves of the determination for 50

μM MP at GR-MWCNTs-COOH/ZrO₂/GCE sensor. The potential value shown in **Fig. 6 (c)** presents a downward trend as the pH value increases, and the linear equation between pH value and peak potential is $E_{\text{pa}1} = -0.054\text{pH} + 0.271$ ($R^2 = 0.998$).

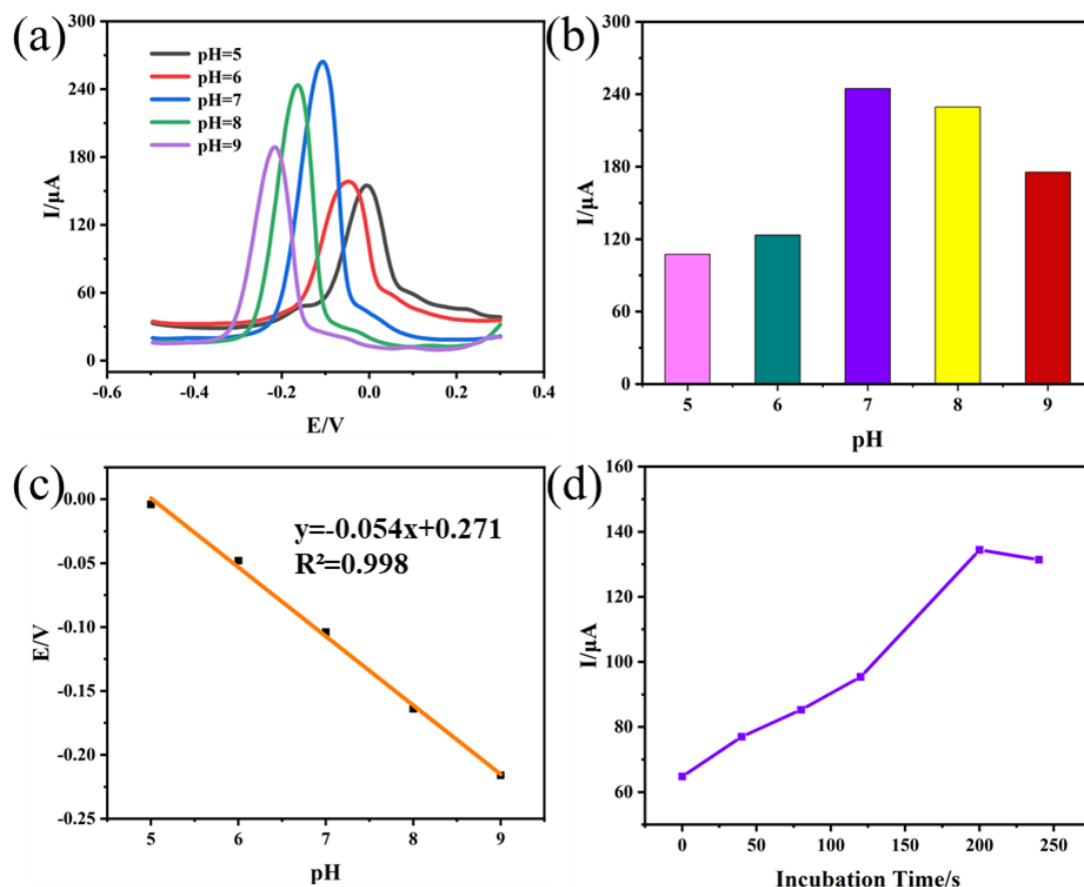


Figure 6. (a) Influence of pH value on the DPV of 50 μM MP at GR-MWCNTs-COOH/ZrO₂/GCE sensor, (b) relationship between pH value and peak current, (c) relationship between pH value and peak potential, and (d) relationship between incubation time and peak current.

The slope of the linear equation is 54 mV/pH, which agrees with the Nernstian value of 58.5 mV/pH, suggesting the detection reaction of MP involves the equal number of electrons and protons at the GR-MWCNTs-COOH/ZrO₂/GCE sensor, which can be confirmed by the reported works [30, 34]. **Fig. 6 (b)** shows the relationship between pH value and peak current. It can be found that the GR-MWCNTs-COOH/ZrO₂/GCE sensor shows the highest peak current value when the pH value is 7.0. This phenomenon has much to do with the effect of pH value on the MP determination. The acidic solution is beneficial to generate more hydroxylamine groups, but it inhibits the generation of nitrosamines (**Scheme 1 b**), which has a negative impact on the transmission of electrons; the alkaline solution is not conducive to reduction of nitro groups to hydroxylamine groups (**Scheme 1 a**), which causes the fact that fewer electrons are transferred in the oxidation reaction [32, 35]. Neither acidic nor alkaline environments are suitable for detecting MP at the GR-MWCNTs-COOH/ZrO₂/GCE sensor. Therefore, pH=7.0 is the suitable experimental condition for the MP detection.

Fig. 6 (d) shows the influence of incubation time on the peak current of MP determination at GR-MWCNTs-COOH/ZrO₂/GCE sensor. It could be found that the incubation of MP molecules reaches to the saturation status on the modified electrode surface when the incubation time is 200s. And the peak current value does not present distinct change with the further increasing of incubation time. Therefore, the incubation time of 200s was applied for the determination of MP.

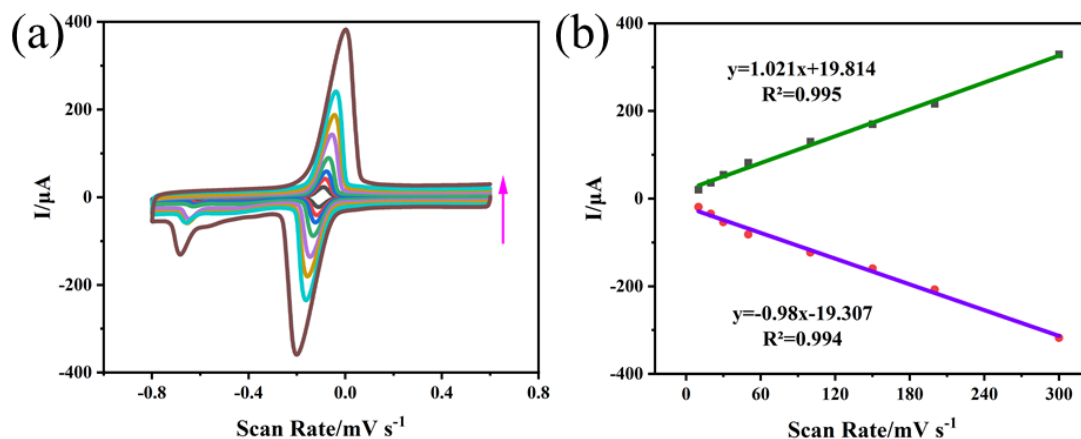


Figure 7. (a) Influence of scanning rate on the CV curves of MP at the GR-MWCNTs-COOH/ZrO₂/GCE sensor and (b) relationship between scanning rate and peak current.

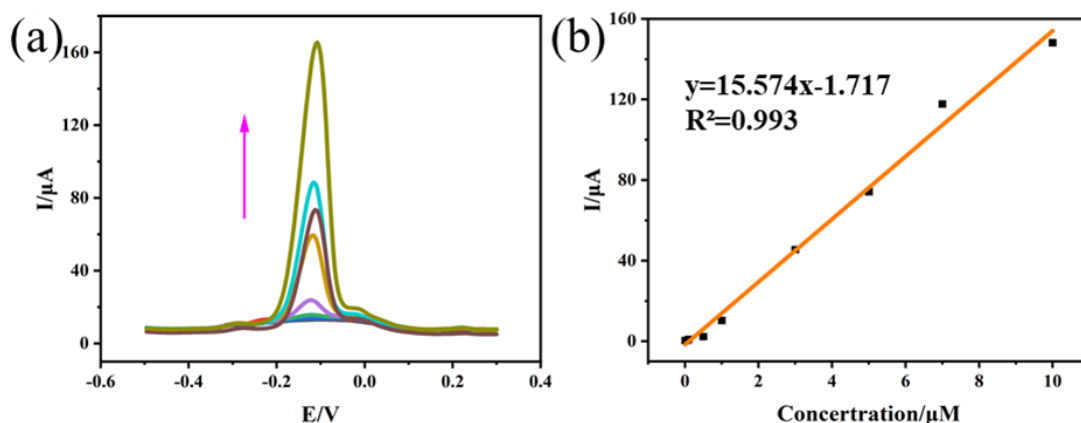


Figure 8. Influence of MP concentration on the DPV curve of MP at the GR-MWCNTs-COOH/ZrO₂/GCE sensor and (b) relationship between MP concentration and oxidation peak (Concentration range: 0.01, 0.05, 0.1, 0.5, 1.0, 3.0, 5.0, 7.0, and 10 μM).

The influence of scanning rate on the determination performance of MP at the GR-MWCNTs-COOH/ZrO₂/GCE sensor was further explored. **Fig. 7 (a)** shows the effect of scanning rate on the CV curves of 30 μM MP (Scanning rate: 0.01-0.3 mV s⁻¹). It can be seen that both oxidation peaks current and reduction peaks current increase with the increasing of scanning rate. **Fig. 7 (b)** shows the relationship between scanning rate and peak current. The corresponding linear regression equations are

described as $I_{pa5}(\mu A) = 1.021v + 19.814$ ($R^2=0.995$) and $I_{pc5}(\mu A) = -0.98v - 19.307$ ($R^2=0.994$), which suggests the detection for MP is an adsorption-controlled process at the GR-MWCNTs-COOH/ZrO₂/GCE sensor.

Fig. 8 (a) shows the influence of MP concentration on the DPV curve of MP at the GR-MWCNTs-COOH/ZrO₂/GCE sensor. The corresponding concentration is 0.01, 0.05, 0.1, 0.5, 1.0, 3.0, 5.0, 7.0, and 10 μM . With the increasing of MP concentration, the oxidation peak value of MP determination shows a gradual increasing trend. **Fig. 8 (b)** exhibits the linear relationship between MP concentration and oxidation peak value. The corresponding linear regression equation is described as $I_{p1}(\mu A) = 15.574C - 1.717$ ($R^2=0.999$). According to the calculation result, the GR-MWCNTs-COOH/ZrO₂/GCE sensor shows a lower limit of detection of 0.00135 μM ($S/N=3$). This phenomenon mainly benefits from the synergistic effect of GR-MWCNTs-COOH and ZrO₂ nanoparticles. GR-MWCNTs-COOH had high electrical conductivity, large specific surface area, and good hydrophilicity, which provide more efficient charge transfer channels and larger electrochemical active area [19-21]; ZrO₂ nanoparticles possessed strong affinity toward the phosphorus groups on MP molecules, which contributes to the enrichment of MP on the GR-MWCNTs-COOH/ZrO₂/GCE sensor [29, 30].

In order to confirm the MP detection performance of GR-MWCNTs-COOH/ZrO₂/GCE sensor, **Table 1** lists the MP determination performance of GR-MWCNTs-COOH/ZrO₂/GCE sensor and other reported sensors. In comparison, the GR-MWCNTs-COOH/ZrO₂/GCE sensor has lower limit of detection, which suggests the good selectivity. Moreover, the cost of fabricated sensor is low, and the preparation process of fabricated sensor does not involve the complicated procedure. Therefore, the GR-MWCNTs-COOH/ZrO₂/GCE sensor has great potential in the field of MP determination.

Table 1. MP determination performance of different MP electrochemical sensors.

Electrode materials	Limit of detection (μM)	Range of linear (μM)	Reference
h-CNT- μ Ps/Nafion/GCE	0.092	0.3-20.0 20.0-150.0	[36]
ERGO-CS/Hb/FTO	0.080	0.076-0.988	[37]
MWCNT/zirconia	0.009	19.9-176.8	[17]
Zr-CNT/GCE	0.243	0.3-34.3	[38]
boron-doped diamond (BDD)	6	0.125-2.0	[39]
AC-GCE	0.0025	1-6	[40]
GR-MWCNTs-COOH/ZrO ₂ /GCE	0.00135	0.01-10	This work

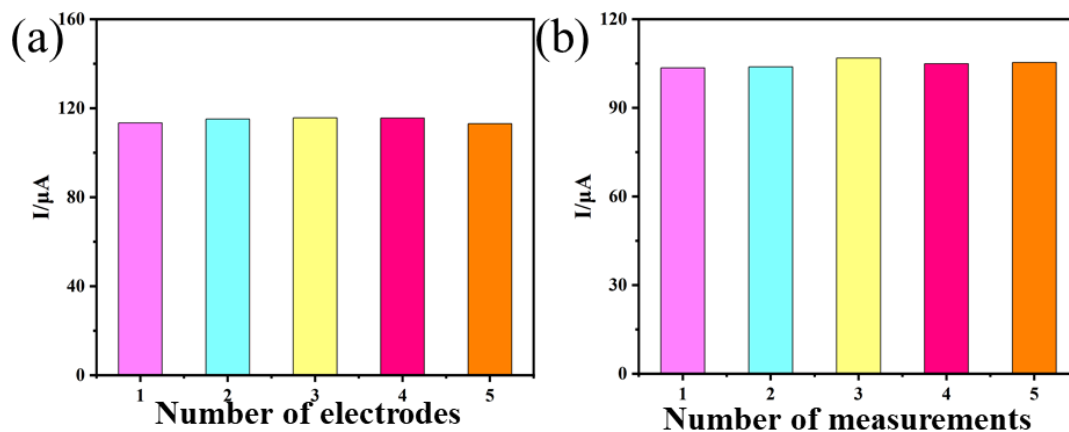


Figure 9. (a) reproducibility and (b) repeatability of the GR-MWCNTs-COOH/ZrO₂/GCE sensor.

Reproducibility and repeatability are also important factors affecting the electrochemical sensing performance. **Fig. 9** shows the reproducibility and repeatability of the GR-MWCNTs-COOH/ZrO₂/GCE sensor. As shown in **Fig. 9(a)**, the peak current values of these GR-MWCNTs-COOH/ZrO₂/GCE sensors has no obvious change. The relative standard deviation (RSD) values of reproducibility and repeatability at GR-MWCNTs-COOH/ZrO₂/GCE sensor are 1.12% and 0.96%, suggesting the good reproducibility and repeatability.

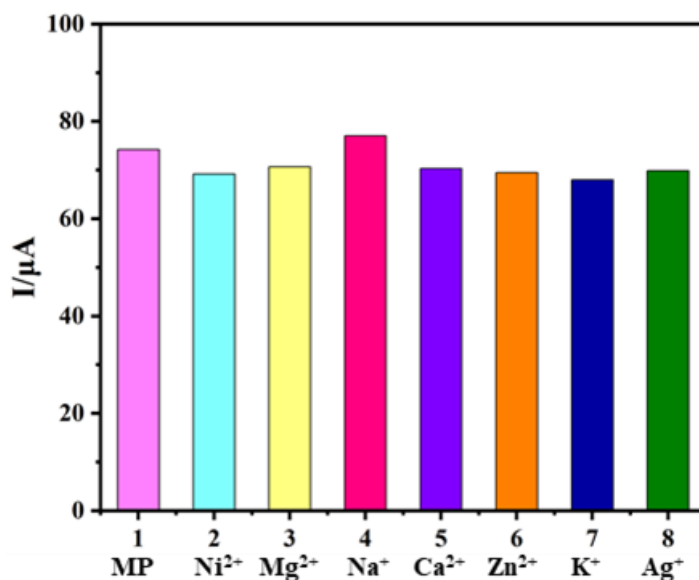


Figure 10. Influence of interfering substances on the detection of MP at the GR-MWCNTs-COOH/ZrO₂/GCE sensor.

Fig. 10 shows the influence of interfering substances on the detection of MP at the GR-MWCNTs-COOH/ZrO₂/GCE sensor. The selectivity measurement was performed by adding the

interfering substances (100-fold MP concentration) including Ag^+ , Na^+ , K^+ , Mg^{2+} , Ni^{2+} , Cu^{2+} and Zn^{2+} . It can be seen that the interfering substances have little effect on the detection of MP at GR-MWCNTs-COOH/ZrO₂/GCE sensos. The corresponding RSD value of GR-MWCNTs-COOH/ZrO₂/GCE sensor is 3.95%, suggesting the good selectivity.

To confirm the practicability of the GR-MWCNTs-COOH/ZrO₂/GCE sensor, two real samples (tap water and lake water) were first filtered by using a standard 0.22 μm filter and then spiked with MP standard solutions. All samples were measured for three times. The recovery of MP in each water sample is the average value of three measured concentration. **Table 2** lists the analytical result of MP in real samples using the proposed sensor. It can be found that the GR-MWCNTs-COOH/ZrO₂/GCE sensor presents satisfactory recoveries of 96.14%-100.27% and relative standard deviation (RSD) values of 1.860-4.173, which suggest the good practicability of the proposed sensor for the MP determination in real samples.

Table 2. Analytical results of MP in real samples using the GR-MWCNTs-COOH/ZrO₂/GCE sensor.

Sample	MP added (μM)	MP found (μM)	Recovery (%)	RSD (%)
Tap water	5.00	4.81	96.14	3.24
	10.00	9.74	97.36	1.86
Lake water	5.00	5.01	100.27	3.25
	10.00	9.65	9.648	4.17

4. CONCLUSION

To summary, we prepared the GR-MWCNTs-COOH/ZrO₂/GCE sensor for the sensitive determination of MP. The synergistic combination of GR-MWCNTs-COOH and ZrO₂ nanoparticles effectively enhanced the MP determination performance. Under optimal conditions, the GR-MWCNTs-COOH/ZrO₂/GCE sensor showed satisfactory linear relationship and low limit of detection of 0.00135 μM . Furthermore, the good reproducibility, repeatability, and selectivity could be obtained at the fabricated sensor, which suggests the good application prospect for the MP determination.

ACKNOWLEDGEMENTS

This work was financially supported by the Natural Science Foundation of Henan Province (No. 202300410163) and University Students' Innovation and Pioneering Project of Henan Province (No. S202110467037X).

References

1. C.S. Pundir, A. Malik and Preety, *Biosens. Bioelectron.*, 140 (2019) 111348.
2. T.H.V. Kumar, S.K. Raman Pillai, M.B. Chan-Park and A.K. Sundramoorthy, *J. Mater. Chem. C*, 8 (2020) 8864.

3. R. Thota and V. Ganesh, *Sensor. Actuat. B: Chem.*, 227 (2016) 169.
4. Chansi, P.R. R, I. Mukherjee, T. Basu and L.M. Bharadwaj, *Nanoscale*, 12 (2020) 21719.
5. F.C. Shaffo, A.C. Grodzki, E.S. Schelegle and P.J. Lein, *Toxicol. Sci.*, 165 (2018) 244.
6. C.G. Zambonin, M. Quinto, N. De Vietro and F. Palmisano, *Food Chem.*, 86 (2004) 269.
7. K. Seebunrueng, Y. Santaladchaiyakit, P. Soisungnoen and S. Srijaranai, *Anal. Bioanal. Chem.*, 401 (2011) 1703.
8. C. Fanali, L. Dugo, P. Dugo and L. Mondello, *TrAC Trend. Anal. Chem.*, 52 (2013) 226.
9. J.L. Armstrong, R.L. Dills, J. Yu, M.G. Yost and R.A. Fenske, *J. Environ. Sci. Health. B*, 49 (2014) 102.
10. G. Cinelli, P. Avino, I. Notardonato and M.V. Russo, *Anal. Methods*, 6 (2014) 782.
11. Q. Wu, Y. Li, C. Wang, Z. Liu, X. Zang, X. Zhou and Z. Wang, *Anal. Chim. Acta*, 638 (2009) 139.
12. H.V.S. Ganesh, B.R. Patel, H. Fini, A.M. Chow and K. Kerman, *Anal. Chem.*, 91 (2019) 10116.
13. A. Venkadesh, J. Mathiyarasu, S. Dave and S. Radhakrishnan, *Inorg. Chem. Commun.*, 131 (2021) 108779.
14. H. Huang, Y. Chen, Z. Chen, J. Chen, Y. Hu and J.J. Zhu, *J. Hazard. Mater.*, 416 (2021) 125895.
15. T. Tao, Y. Zhou, C. He, H. He, M. Ma, Z. Cai, N. Gao, K. Wang, R. Zhu, G. Chang, Z. Liu and Y. He, *Electrochim. Acta*, 357 (2020) 136836.
16. Z. Liang, H. Zhai, Z. Chen, H. Wang, S. Wang, Q. Zhou and X. Huang, *Sensor. Actuat. B: Chem.*, 224 (2016) 915.
17. K.d.S. Caetano, D.S. da Rosa, T.M. Pizzolato, P.A.M. dos Santos, R. Hinrichs, E.V. Benvenuti, S.L.P. Dias, L.T. Arenas and T.M.H. Costa, *Micropor. Mesopor. Mat.*, 309 (2020) 110583.
18. B. Huang, W.-D. Zhang, C.-H. Chen and Y.-X. Yu, *Microchim. Acta*, 171 (2010) 57.
19. S. Zhang, Y. Shao, G. Yin and Y. Lin, *Appl. Catal. B: Environ.*, 102 (2011) 372.
20. Y. Xue, S. Zheng, Z. Sun, Y. Zhang and W. Jin, *Chemosphere*, 183 (2017) 156.
21. C. Singh, S. Srivastava, M.A. Ali, T.K. Gupta, G. Sumana, A. Srivastava, R.B. Mathur and B.D. Malhotra, *Sensor. Actuat. B: Chem.*, 185 (2013) 258.
22. J. Li, D. Kuang, Y. Feng, F. Zhang and M. Liu, *Microchim. Acta*, 172 (2010) 379.
23. M. Ni, J. Chen, C. Wang, Y. Wang, L. Huang, W. Xiong, P. Zhao, Y. Xie and J. Fei, *Microchem. Journal*, 178 (2022) 107410.
24. K. Prabhu, S.J. Malode and N.P. Shetti, *Environ. Technol. Inno.*, 23 (2021) 101687.
25. S. Đurđić, V. Stanković, F. Vlahović, M. Ognjanović, K. Kalcher, D. Manojlović, J. Mutić and D.M. Stanković, *Microchem. J.*, 168 (2021) 106416.
26. J. Upan, N. Youngvises, A. Tuantranont, C. Karuwan, P. Banet, P.H. Aubert and J. Jakmune, *Sci. Rep.*, 11 (2021) 13969.
27. H. Zhao, H. Ma, X. Li, B. Liu, R. Liu and S. Komarneni, *Appl. Clay Sci.*, 200 (2021) 105907.
28. Y. Zhou, T. Wu, H. Zhang, M. Zhao, Y. Shen, G. Zhu, M. Guo, Y. Liu, F. Li, and H. Zhao, *Int. J. Electrochem. Sci.*, doi: 10.20964/2022.06.50.
29. H. Zhao, B. Liu, Y. Li, B. Li, H. Ma and S. Komarneni, *Ceram. Int.*, 46 (2020) 19713.
30. J. Gong, X. Miao, H. Wan and D. Song, *Sensor. Actuat. B-Chem.*, 162 (2012) 341.
31. A.R. Tobi, J.O. Dennis, H.M. Zaid, A.A. Adekoya, A. Yar and U. Fahad, *J. Mater. Res. Technol.*, 8 (2019) 3688.
32. H. Zhao, B. Li, R. Liu, Y. Chang, H. Wang, L. Zhou and S. Komarneni, *Mater. Sci. Eng. C Mater. Biol. Appl.*, 123 (2021) 111982.
33. H. Zhao, Y. Chang, R. Liu, B. Li, F. Li, F. Zhang, M. Shi, L. Zhou and X. Li, *Food. Chem.*, 343 (2021) 128484.
34. Y. Yao, L. Zhang, J. Xu, X. Wang, X. Duan and Y. Wen, *J. Electroanal. Chem.*, 713 (2014) 1.
35. X. Dong, F. Wang, J. Ma, and B. Qiu, *Int. J. Electrochem. Sci.*, 14 (2019) 11679.
36. J. Yao, Z. Liu, M. Jin, Y. Zou, J. Chen, P. Xie, X. Wang, E.M. Akinoglu, G. Zhou and L. Shui, *Sensor. Actuat. B: Chem.*, 321 (2020) 128517.
37. R. Kaur, S. Rana, K. Lalit, P. Singh and K. Kaur, *Biosens. Bioelectron.*, 167 (2020) 112486.

38. K.P. Gannavarapu, V. Ganesh and R.B. Dandamudi, *Nanoscale Adv.*, 1 (2019) 4947.
39. P.A.R. de Sousa, A.L. Squizzato, R.A.A. Munoz, L.M. Coelho, E.I. de Melo and R.A.B. da Silva, *Anal. Methods*, 12 (2020) 5801.
40. M. Stoycheva, R. Zlatev, Z. Velkova, V. Gochev, G. Montero, B. Valdez and M. Curiel, *Electroanal.*, 33 (2020) 438

© 2022 The Authors. Published by ESG (www.electrochemsci.org). This article is an open access article distributed under the terms and conditions of the Creative Commons Attribution license (<http://creativecommons.org/licenses/by/4.0/>).